

## Supplementary Information for

### **Biocompatible and Stable Quasi-solid-state Zinc-ion Batteries for Real-time Responsive Wireless Wearable Electronics**

Bingyao Zhang,<sup>a, ‡</sup> Xinze Cai,<sup>b, ‡</sup> Jingjing Li,<sup>c</sup> Hao Zhang,<sup>d</sup> Dongmin Li,<sup>a</sup> Haoyang Ge,<sup>a</sup>

Shuquan Liang,<sup>a</sup> Bingan Lu,<sup>c</sup> Jiangqi Zhao,<sup>b, \*</sup> Jiang Zhou<sup>a, \*</sup>

*a. School of Materials Science and Engineering, Hunan Provincial Key Laboratory of Electronic Packaging and Advanced Functional Materials, Central South University, Changsha 410083, China, E-mail: zhou\_jiang@csu.edu.cn.*

*b. College of Materials Science and Engineering, Sichuan University, Chengdu 610065, China, E-mail: jiangqizhao@scu.edu.cn.*

*c. Department of Plastic Surgery and National Clinical Research Center for Geriatric Disorders, Xiangya Hospital, Central South University, Changsha 410008, China.*

*d. Chemistry Research Laboratory, Department of Chemistry, University of Oxford, Oxford OX1 3TA, UK.*

*e. School of Physics and Electronics, Hunan University, Changsha 410082, China.*

*‡ These authors contributed equally: Bingyao Zhang, Xinze Cai.*

*\* These authors jointly supervised this work: Jiangqi Zhao, Jiang Zhou. Email: Jiangqi Zhao, jiangqizhao@scu.edu.cn; Jiang Zhou, zhou\_jiang@csu.edu.cn*

## Methods

### Preparation of Ur-SA, SAZC, AAK and PVLF hydrogel electrolytes

The quasi-solid urea modified sodium alginate composite hydrogel electrolyte (Ur-SA) was synthesized by simply mixing 10 g urea (AR grade, Macklin), 2 g sodium alginate (AR grade, Macklin) and 60 mL deionized water. The mixed solution then was vacuum stirred at room temperature for 12 h to make it as uniform as possible, then immersed in the mixed solution of 0.1 mol/L  $\text{MnSO}_4$  and 2 mol/L  $\text{ZnSO}_4$  overnight in a glass petri plate for cross-linking process to obtain the resultant Ur-SA hybrid hydrogel.

SA hydrogel immersed in  $\text{ZnCl}_2$  solution (SAZC) was obtained by a straightforward procedure of blending 2 g of sodium alginate (AR grade, Macklin) with 60 mL of deionized water. The mixture was vigorously stirred under a vacuum at room temperature for 12 hours to ensure uniformity. Subsequently, the solution was immersed in a glass petri plate containing 0.5 mol/L  $\text{ZnCl}_2$  and left overnight for the cross-linking process to acquire the ultimate SAZC hydrogel.

Polyacrylic acid-based hydrogel electrolyte (AAK) was synthesized through a straightforward process of thermal polymerization. 7.2 mL of acrylic acid was slowly added to 15 mL of deionized water with continuous stirring until its complete dissolution. Afterwards, 110 mg of ammonium persulfate and 4 mg of N,N'-Methylenebisacrylamide were added and stirred for half an hour. The resulting mixture was poured into a mold and purged with argon gas, then polymerized at 65°C for half an hour. After the polymerization, the hydrogel was dried in an 80°C oven and subsequently immersed in a mixture of 0.6 M zinc acetate and 6 M KOH solution to obtain the resultant AAK hydrogel.

PVDF-based organic hydrogel electrolyte (PVLF) was prepared by dissolving 1.5g of PVDF in 20mL of DMF (N,N-dimethylformamide) at 55°C with stirring for 3 hours. The resulting solution was then poured into a mold and subjected to vacuum drying at 50°C for 12 hours. After that, the dried PVDF film was immersed in a 1M lithium hexafluorophosphate [ $\text{LiPF}_6$ -EC: DMC: EMC (1:1:1)] solution for 2 hours to acquire the final PVLF hydrogel.

## **Synthesis of MnO<sub>2</sub>**

3 mmol MnSO<sub>4</sub> and 2 mL 0.5 M H<sub>2</sub>SO<sub>4</sub> were added to 90 mL deionized water with magnetic stirring to obtain a clear solution. Then, 20 mL 0.1 M KMnO<sub>4</sub> aqueous solution was slowly added to the above solution. The mixture was stirred for 2 h at room temperature and then transferred into a Teflon-lined autoclave and heated at 120 °C for 12 h. Ultimately, the obtained MnO<sub>2</sub> powder was washed repeatedly with distilled water and dried at 60 °C in a vacuum oven.

## **Materials characterizations**

Phase analyses and the crystal structures of the samples were investigated by X-ray diffraction (XRD) (Rigaku Mini Flex 600 diffractometer, Cu K $\alpha$  radiation,  $\lambda = 1.5418 \text{ \AA}$ ) with a scan rate of  $10^\circ \text{ min}^{-1}$  at the step size of  $0.02^\circ$ . The morphologies and the elemental distribution were characterized by a field emission scanning electron microscope (FESEM, FEI Nova NanoSEM 230, 10 kV) equipped with an energy dispersive spectrometer (EDS). Fourier Transform Infrared Spectroscopy (FTIR) spectra were measured by Nicolet 6700. X-ray photoelectron spectra (XPS) were obtained by ESCALAB 250 Xi X-ray photoelectron spectrometer (Thermo Fisher). Thermogravimetric (TG) analysis was performed on a Mettler Toledo TGA/DSC1 with a heating rate of  $10^\circ \text{ C min}^{-1}$  in the Ar atmosphere (Netzsch STA 449 C).

## **Electrochemical characterizations**

The cathode slurry for the full cell was fabricated by mixing MnO<sub>2</sub> (70 wt %), Ketjenblack (20 wt %), polyvinylidene fluoride (PVDF, 10 wt %) and N-methyl-2-pyrrolidone (NMP). Then the slurry was uniformly coated onto carbon cloth (CC) and then dried in a vacuum oven at 80 °C for 12 h. CR2025 coin cells were assembled by using MnO<sub>2</sub> cathode, UA-SA, SA, or 2 mol/L ZnSO<sub>4</sub> with 0.1mol/L MnSO<sub>4</sub> liquid electrolyte and Zn anode. The corresponding electrochemical properties at room temperature were measured by a multichannel battery testing system (LAND CT2001A, China). The cyclic voltammetry (CV), chronoamperometry (CA), electrochemical impedance spectroscopy (EIS) spectra and linear sweep voltammetry (LSV) curves were collected by an electrochemical workstation (CHI660E, China). CA investigations were conducted at the potential amplitude of 200 mV and pulse width of 200s.

CV profiles were performed at the scan rate of  $0.1 \text{ mV s}^{-1}$  with a voltage range of 0.8-1.8 V, and then EIS was tested within the frequency range from  $10^{-2}$  to  $10^5$  Hz. LSV measurement is conducted in the three-electrode configuration at room temperature, in which stainless-steel is adopted as a working electrode and Zn foils are used as a counter electrode and reference electrode, respectively.

### **Preparation of printing inks and planar zinc-ion micro-batteries**

The conductive carbon paste was prepared by mixing 80 mg Ketjenblack, 100 mg CNT and 20 mg PVDF in 2000 mg NMP. Then the mixture was intensely stirred for 12 hours, after ultrasonic treatment for 8 hours. Next, the corresponding cathode slurries were prepared by mixing Ketjenblack and PVDF,  $\text{MnO}_2$  and Zn powder in NMP in certain ratios with stirring, respectively.

The planar zinc-ion micro-batteries are prepared by screen-printing. Step one, the ultrasonic-cleaned PET film was fixed between the stencil and the printing table. Secondly, the prepared conductive carbon paste was poured onto one side of the stencil and pushed by the scraper to the other side. Thirdly, the printed interlayer was dried at  $80 \text{ }^\circ\text{C}$  overnight in a vacuum oven. Fourthly,  $\text{MnO}_2$  ink and Zn ink were separately printed on the two sides of the conductive interlayer with the scraper, and fully dried to acquire printed cathodes and anodes, respectively. Step 2, the printed microelectrodes were covered with Ur-SA gel electrolyte and encapsulated with Kapton tape to assemble planar zinc-ion batteries (ZIBs).

### **Assembly of integrated wearable sensing system**

The integrated wearable sensing system was comprised of an energy module, sensing module, controlling module, data transmission module, and display module. The sensor of hydrogel was integrated into a printed circuit board (PCB). The microcontroller unit (STC32G12K128) and Bluetooth module were welded on the PCB and responsible for real-time processing and data transmission, respectively.

The energy module is in the form of a flexible wristband, consisting of three planar ZIBs connected in series. To fabricate resistive-type strain sensors from hydrogels, Ur-SA hydrogel

is tailored into strips (50 mm×10 mm×1 mm) with two outstretching conductive tapes. The two ends of the sensor strips were connected to the PCB to measure the resistance variation. The real-time responsive resistance variation is collected by the software of the Bluetooth serial port on a smartphone.

Strain sensing test of Ur-SA was done by attaching the hydrogel directly to the workstation using p-t mode, the resistance was calculated based on current data in real-time.

### **Biocompatibility and safety research**

This study was conducted in accordance with the guidelines of the Department of Laboratory Animals of Central South University (CSU-2022-0122). Male New Zealand White Rabbits were randomly distributed into four experimental groups and were anesthetized using pentobarbital sodium for intravenous injection. Select the midline dorsal incisions to free the whole back. The back is divided into four regions with the implantation of Ur-SA (experimental group) and SAZC, AAK and PVLf (control group). Then the corresponding hydrogels were implanted subcutaneously in New Zealand white rabbits. After 4 weeks, the implants surrounding tissue were collected and investigated by hematoxylin and eosin (H&E) staining and Masson's trichrome (M&T) staining. All animal procedures were performed in accordance with the Guidelines for Care and Use of Laboratory Animals of Central South University and approved by the Animal Ethics Committee of Department of laboratory animals.

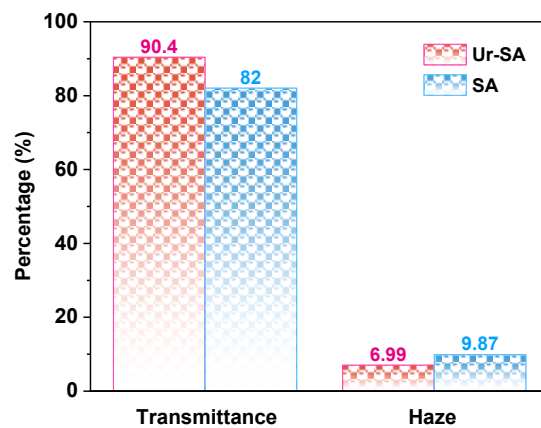


**Fig. S1.** Transmittance spectra of Ur-SA and SA in the visible wavelength range. An average transmittance of over 90.4% and 82.0% was recorded for Ur-SA and SA, respectively.

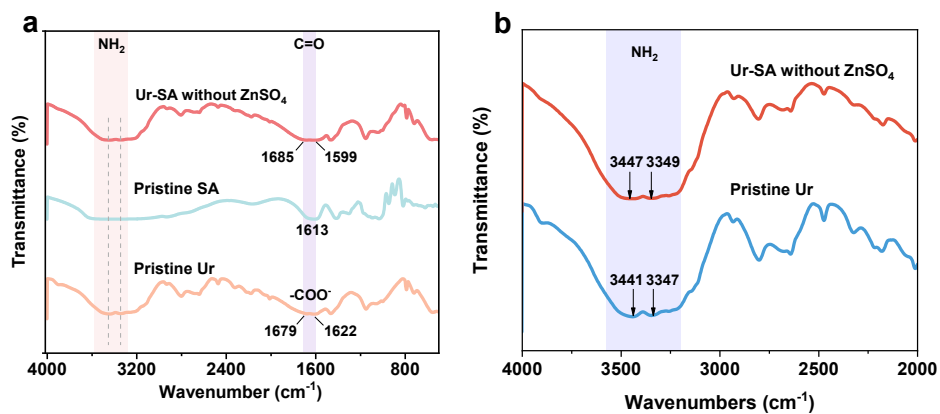


**Fig. S2.** Fourier Transform Infrared Spectroscopy (FTIR) spectra of Ur-SA under various states. (a) FTIR spectra of pristine Ur, pristine SA and Ur-SA without ZnSO<sub>4</sub>. (b) The corresponding enlarged version of FTIR spectra of pristine Ur and Ur-SA without ZnSO<sub>4</sub>.

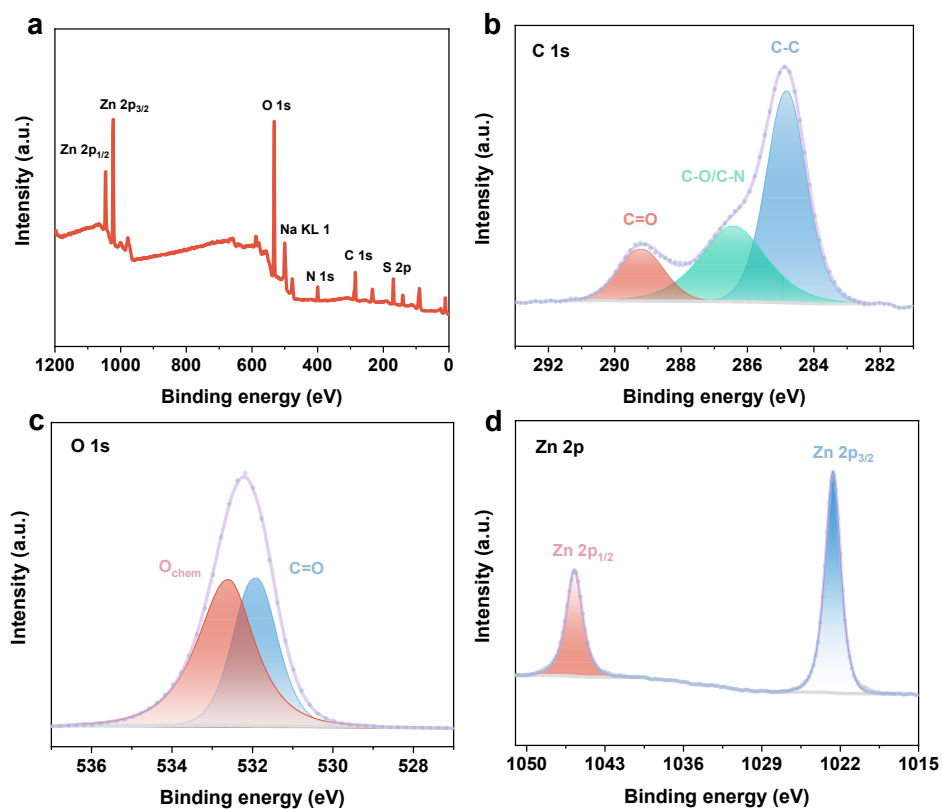


**Fig. S3.** The XPS spectra of Ur-SA immersed in ZnSO<sub>4</sub> electrolyte. (a) The corresponding XPS survey spectrum. High-resolution XPS spectra of (b) C 1s, (c) O 1s and (d) Zn 2p.

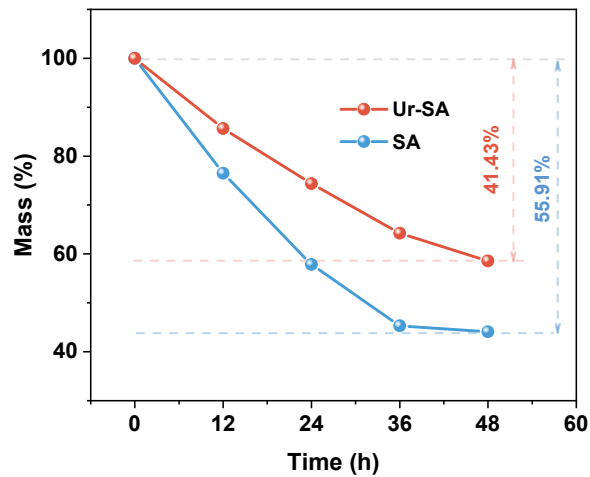


**Fig. S4.** Weight changes of Ur-SA and SA hydrogel electrolytes in ambient atmosphere at room temperature.

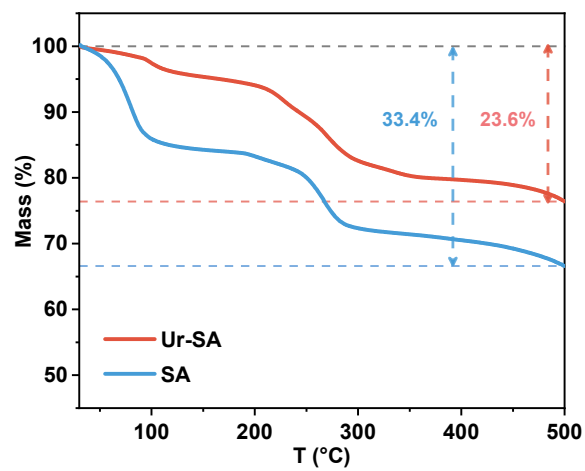


**Fig. S5.** TGA curves of Ur-SA and SA electrolytes.

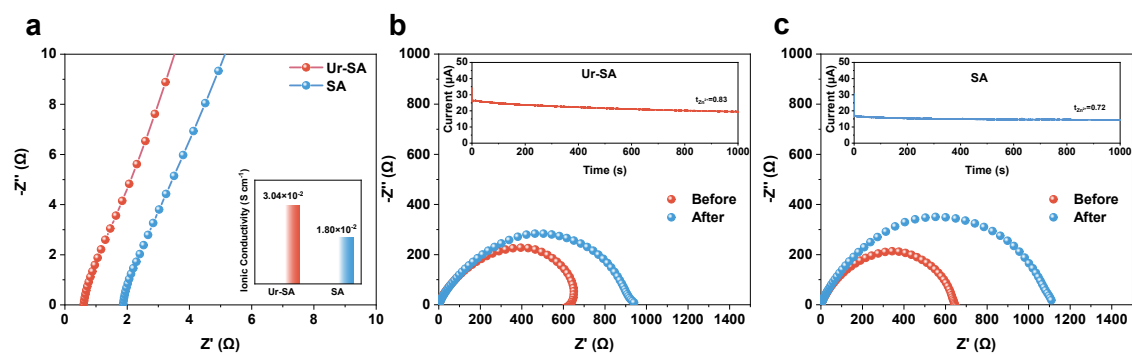


**Fig. S6.** AC impedance spectra based on Ur-SA and SA in the frequency range of 100 kHz to 0.01 Hz for (a) stainless steel-based batteries. EIS spectra of Zn/Zn symmetrical batteries with Ur-SA (b) and SA (c) before and after polarization, inset: the  $i$ - $t$  curve at an applied voltage of 10 mV.

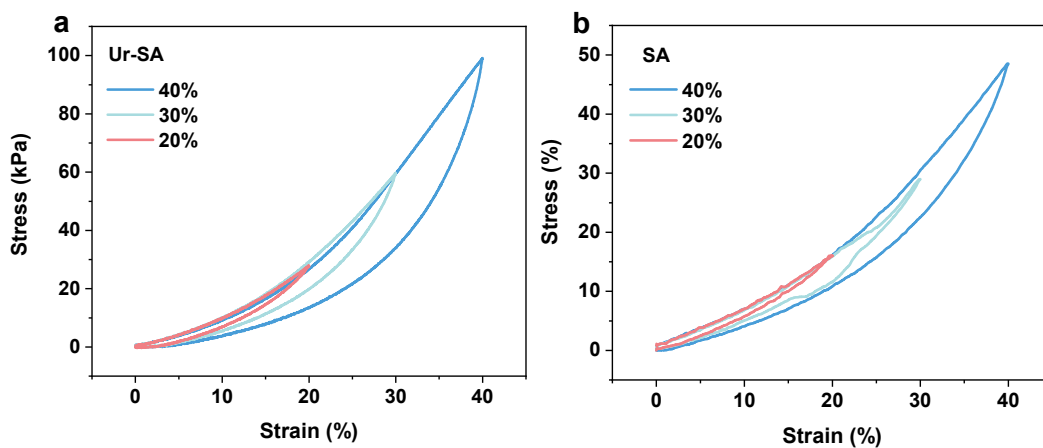


**Fig. S7.** Determining the elasticity property of hydrogels. Compressive stress-strain curves of Ur-SA (a) and SA (b) under various strains.

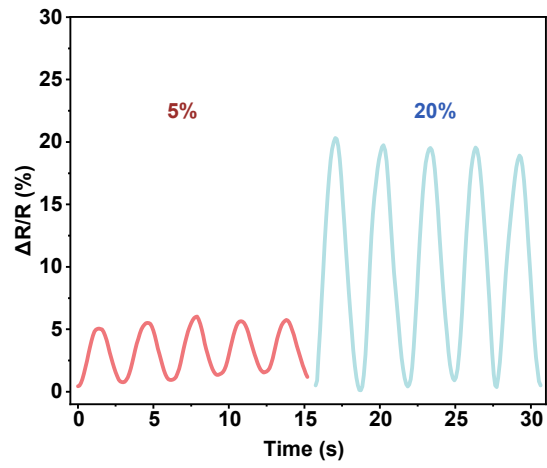


**Fig. S8.** Relative resistance responses of the Ur-SA hydrogel sensor at 0.33 Hz under small cyclical stretches.

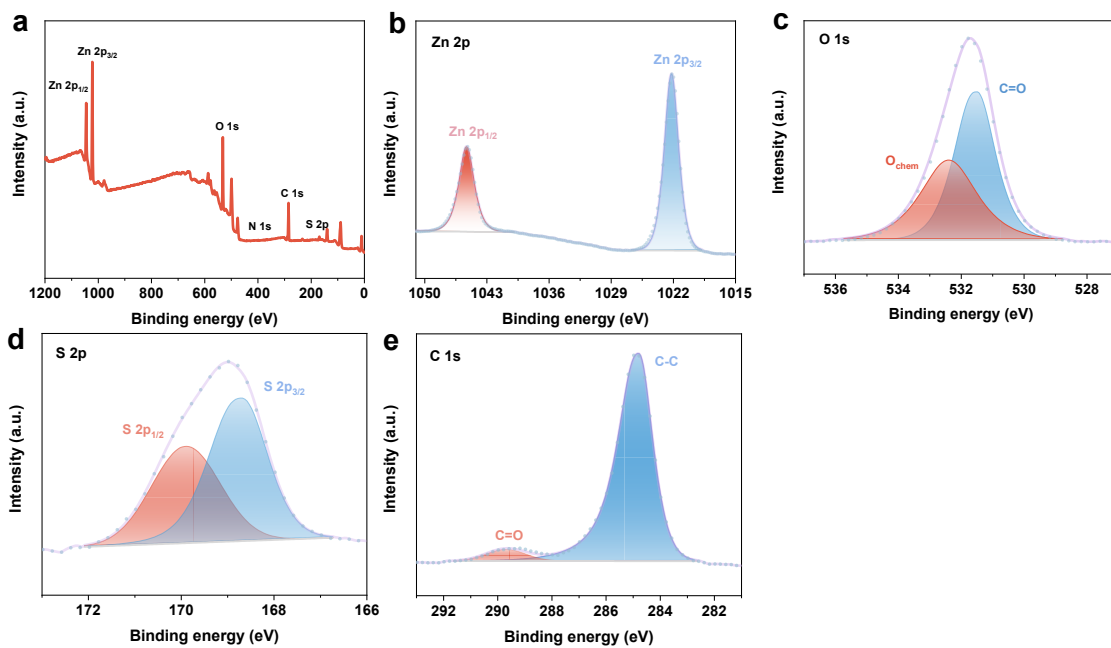


**Fig. S9.** X-ray photoelectron spectroscopy (XPS) survey spectrum of the Zn anode in Zn/Zn symmetric cells after 200 cycles. (a) XPS survey spectrum of Zn anode in Zn/Zn symmetric cells after plating/stripping for 200 cycles at  $0.5 \text{ mA cm}^{-2}$ . High-resolution XPS spectrum of Zn 2p (b), O 1s (c), S 2p (d), C 1s (e).

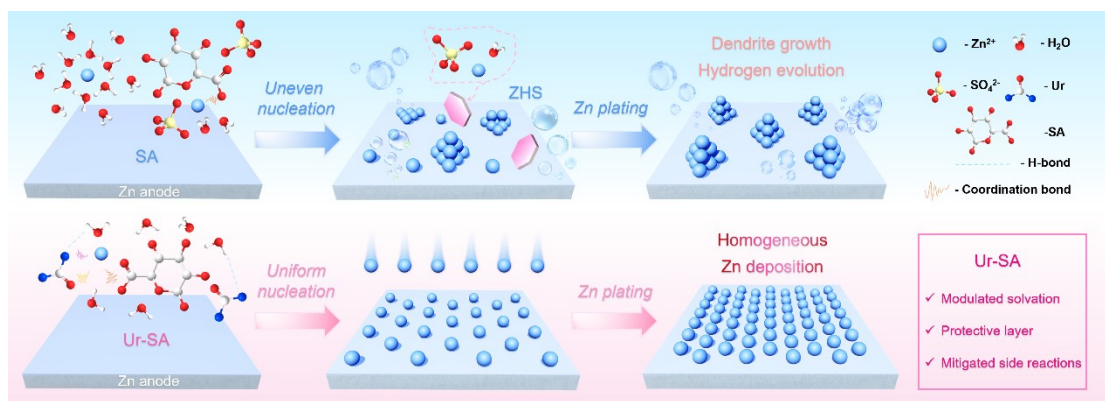


**Fig. S10.** Schematic illustration of Zn deposition in SA (up) and Ur-SA (down) electrolytes.

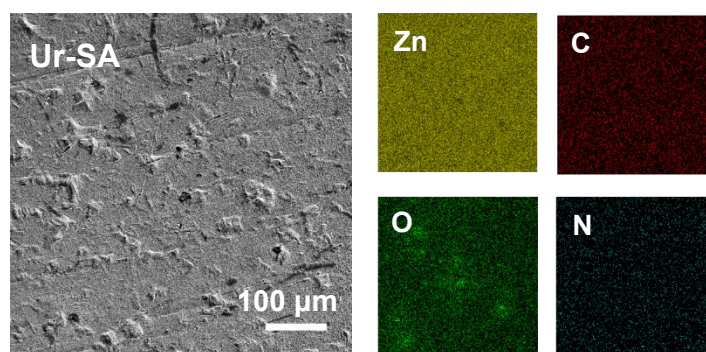


**Fig. S11.** The SEM image and EDS mapping of Zn anode in Zn/Zn symmetric cells after plating/stripping for 200 cycles at  $0.5 \text{ mA cm}^{-2}$ .

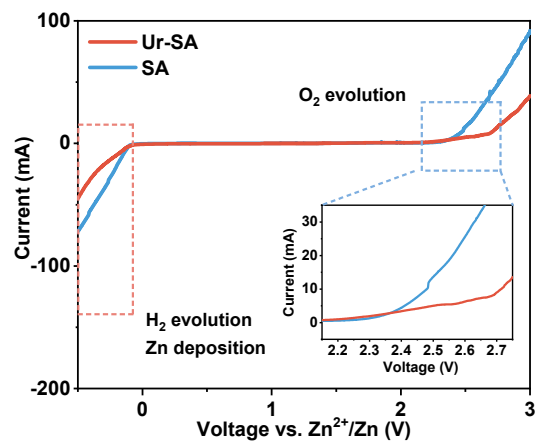


**Fig. S12.** Linear sweep voltammetry curves with a scan rate of  $5 \text{ mV s}^{-1}$  for Ur-SA and SA.

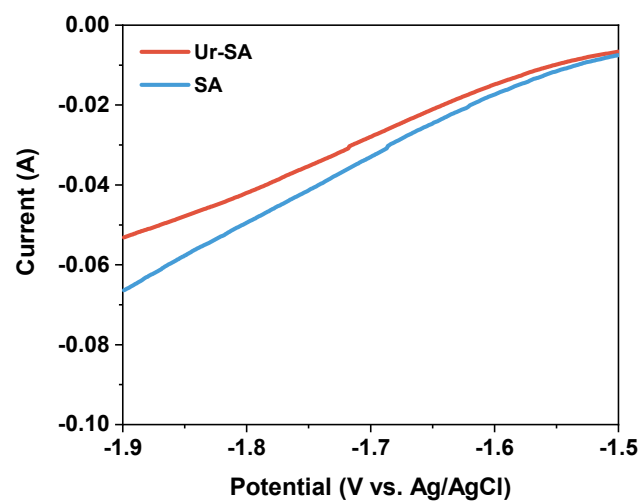


**Fig. S13.** Hydrogen evolution polarization curves of zinc anodes in Ur-SA and SA.

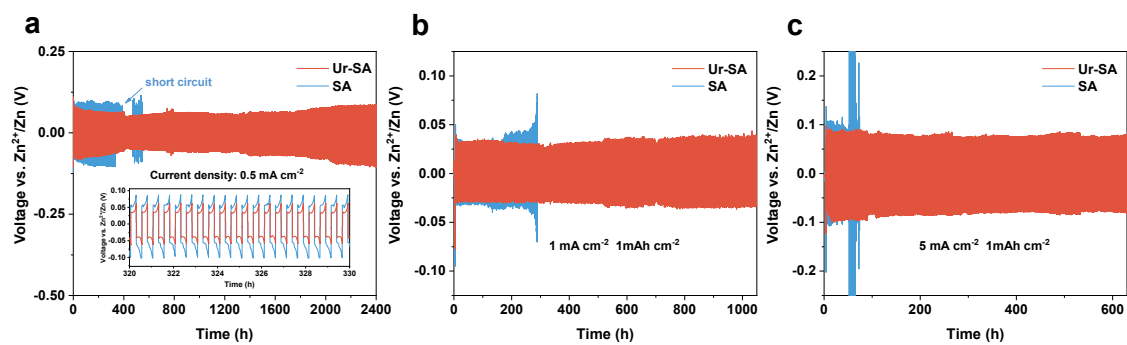


**Fig. S14.** Zn plating/stripping performances of Zn/Zn symmetric cells under a current density of (a)  $0.5 \text{ mA cm}^{-2}$   $0.125 \text{ mAh cm}^{-2}$ , (b)  $1 \text{ mA cm}^{-2}$   $1 \text{ mAh cm}^{-2}$  and (c)  $5 \text{ mA cm}^{-2}$   $1 \text{ mAh cm}^{-2}$  at room temperature.

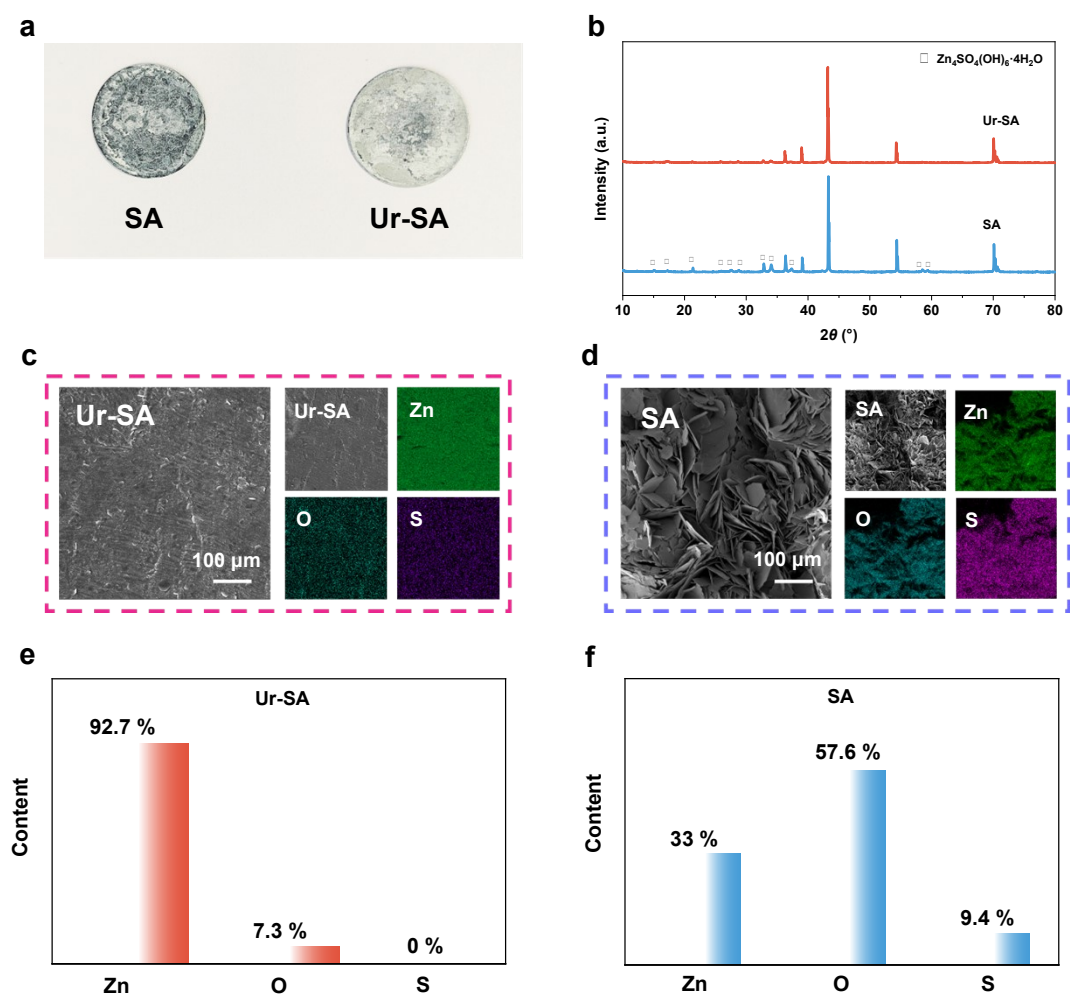


**Fig. S15.** Determining the interface situation of Zn anode after 800 plating/stripping cycles in a Zn/Zn symmetric cell at  $0.5 \text{ mA cm}^{-2}$ . The optical image of Zn metal anodes (a), corresponding XRD patterns (b), the SEM, EDS images and concentration distribution of Zn, O and S of Zn anode surface in Ur-SA (c, e) and SA (d, f).

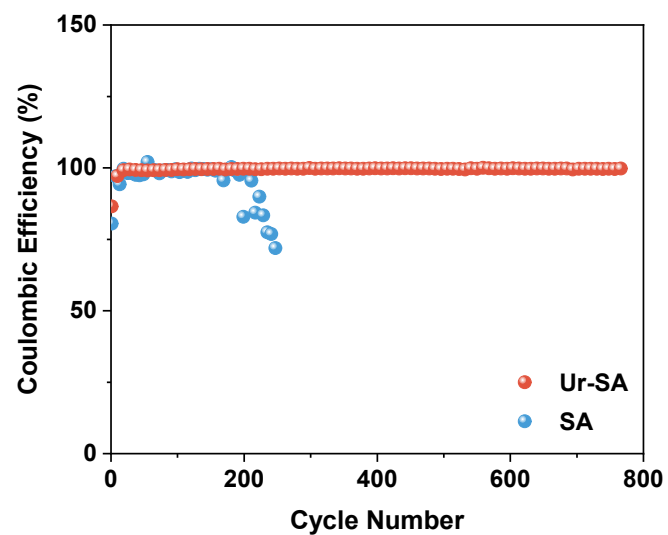


**Fig. S16.** Coulombic efficiency of the Zn/Cu asymmetric cells with Ur-SA and SA at  $1 \text{ mA cm}^{-2}$ ,  $0.5 \text{ mAh cm}^{-2}$ .

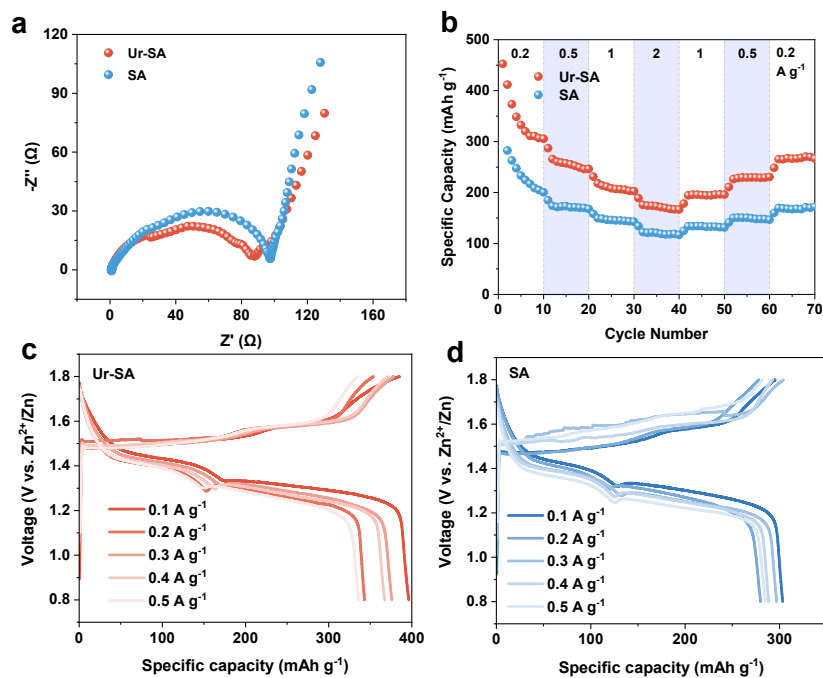


**Fig. S17.** Electrochemical characterization of the Zn/MnO<sub>2</sub> battery using Ur-SA and SA hydrogel electrolyte. (a) AC impedance spectra based on Ur-SA and SA in the frequency range of 100 kHz to 0.01 Hz for Zn/MnO<sub>2</sub> full batteries. (b) The rate capability of the Zn/MnO<sub>2</sub> battery using Ur-SA and SA at various current densities from 0.2 A g<sup>-1</sup> to 2 A g<sup>-1</sup>. Galvanostatic charge/discharge profiles of the Zn/MnO<sub>2</sub> batteries at different current densities from 0.1 A g<sup>-1</sup> to 0.5 A g<sup>-1</sup> with (c) Ur-SA and (d) SA.

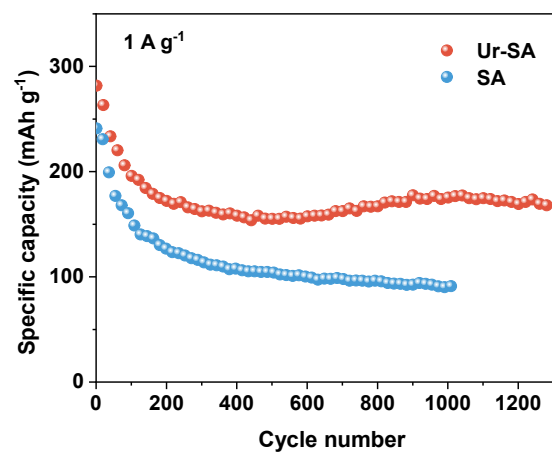


**Fig. S18.** Long-time cycling performance of the Zn/MnO<sub>2</sub> batteries with Ur-SA and SA at 1 A g<sup>-1</sup>.

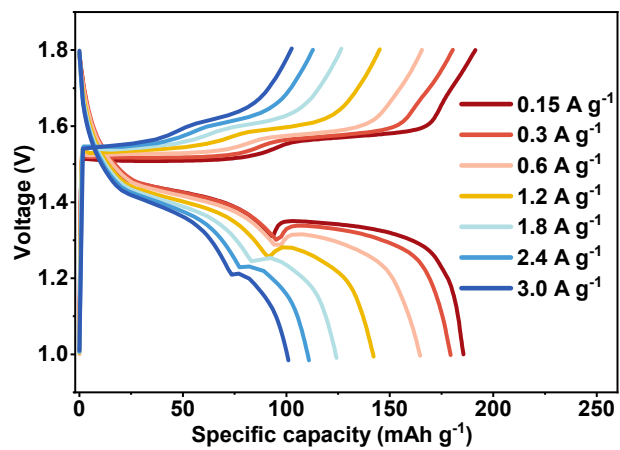


**Fig. S19.** GCD profiles of the planar zinc ion battery (ZIB) at different current densities.

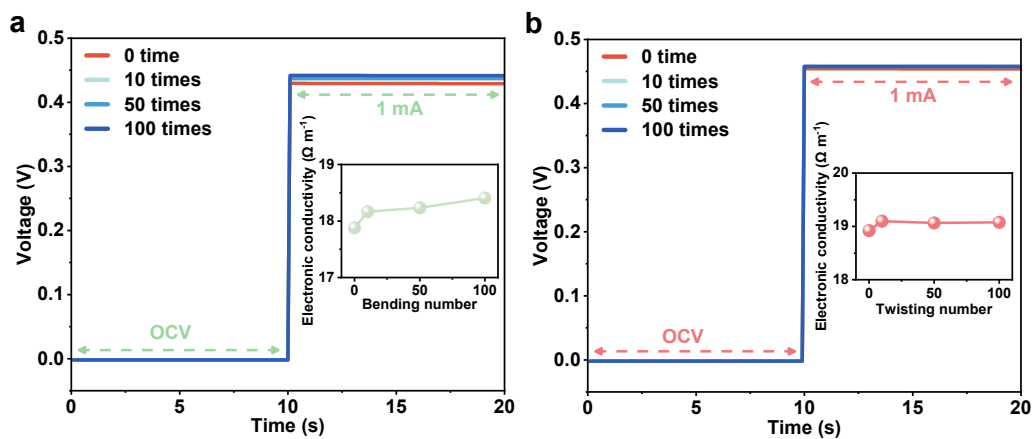


**Fig. S20.** Mechanical stability testing of the printed planar batteries with Ur-SA. Resistivity of the electrodes after (a) being bent for different times or (b) being twisted for different times.

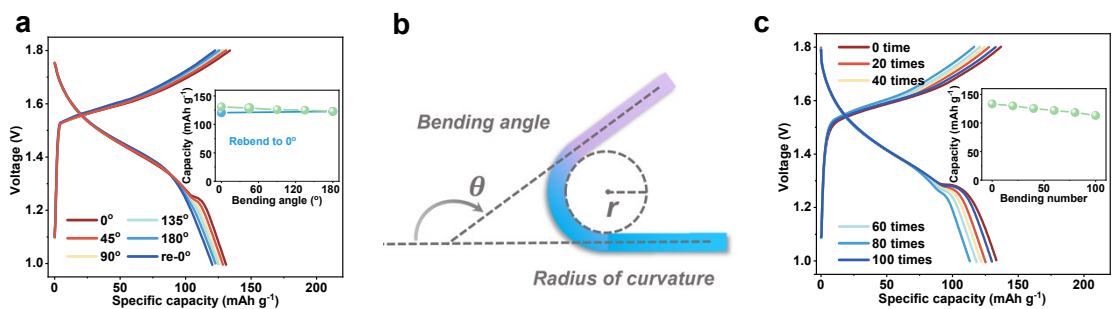


**Fig. S21.** Mechanical stability testing of the printed planar ZIBs (a) The GCD curves under different bending angles. (b) The schematic diagram of different bending states. (c) The GCD curves after different bending times.

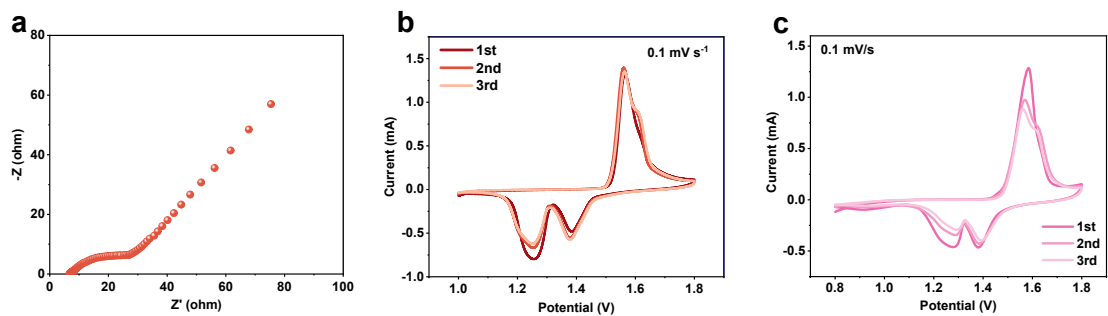


**Fig. S22.** Electrochemical characterization of the printed planar ZIBs (a) EIS spectra of MnO<sub>2</sub>/Ur-SA/Zn planar screen-printed batteries in the frequency range of 100 kHz to 0.01 Hz. (b) Cyclic voltammetry curves of planar batteries with Ur-SA at a scan rate of 0.1 mV s<sup>-1</sup>. (c) Cyclic voltammetry curves of coin cells with Ur-SA at a scan rate of 0.1 mV s<sup>-1</sup>.

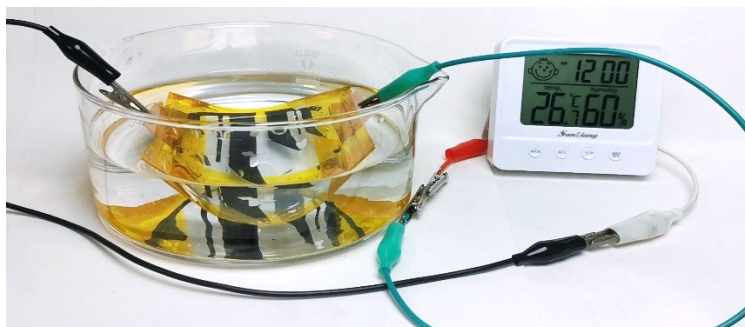


**Fig. S23.** Safety tests of the planar ZIBs under soaking conditions.

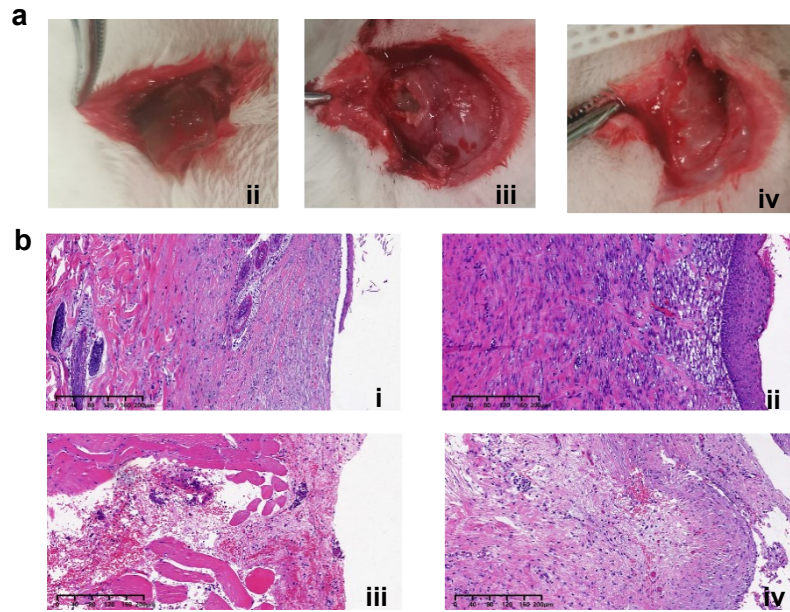


**Fig. S24.** Determining the biocompatibility and internal stability of the implantable hydrogels. (a) Evolution of the implanted hydrogels in the region of the back after 4 weeks. (b) Hematoxylin-eosin (H&E) stain staining of tissues surrounding different hydrogels after implantation for 1 month. Ur-SA, SAZC, AAK and PVLF are presented by i, ii, iii and iv respectively.



**Fig. S25.** Digital photographs demonstrating the integration process of the self-powered wearable sensing system.

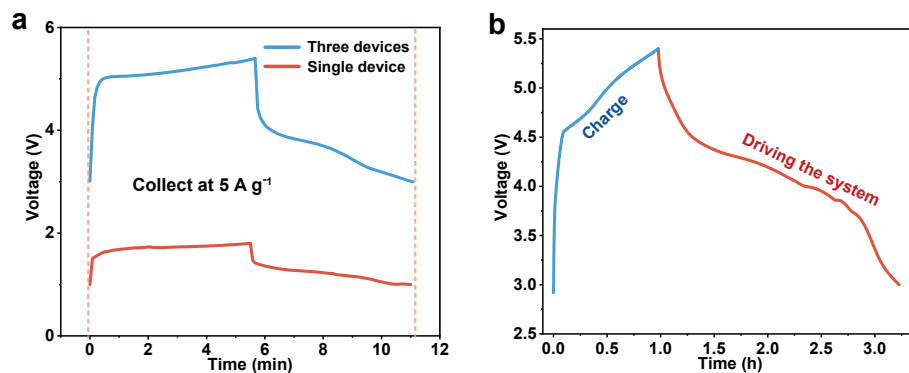


**Fig. S26.** Verifying the feasibility of wearable sensing system driven by the planar ZIBs. (a) The GCD curves of planar ZIBs in parallel and series connections. (b) The curves of the power supply to wearable sensing network by three series-wound planar ZIBs.

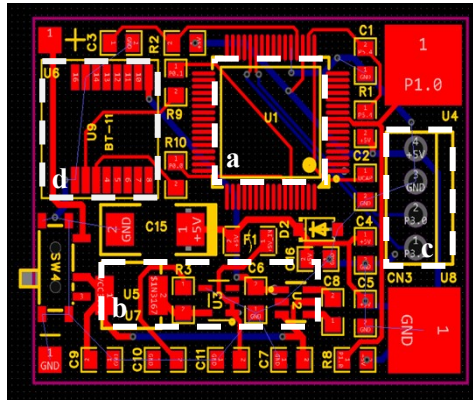


**Fig. S27.** Image of PCB layout design. (a) STC32G12K128 Microcontroller Unit. (b) Power management circuit. (c) Program debugging interface. (d) Bluetooth module.

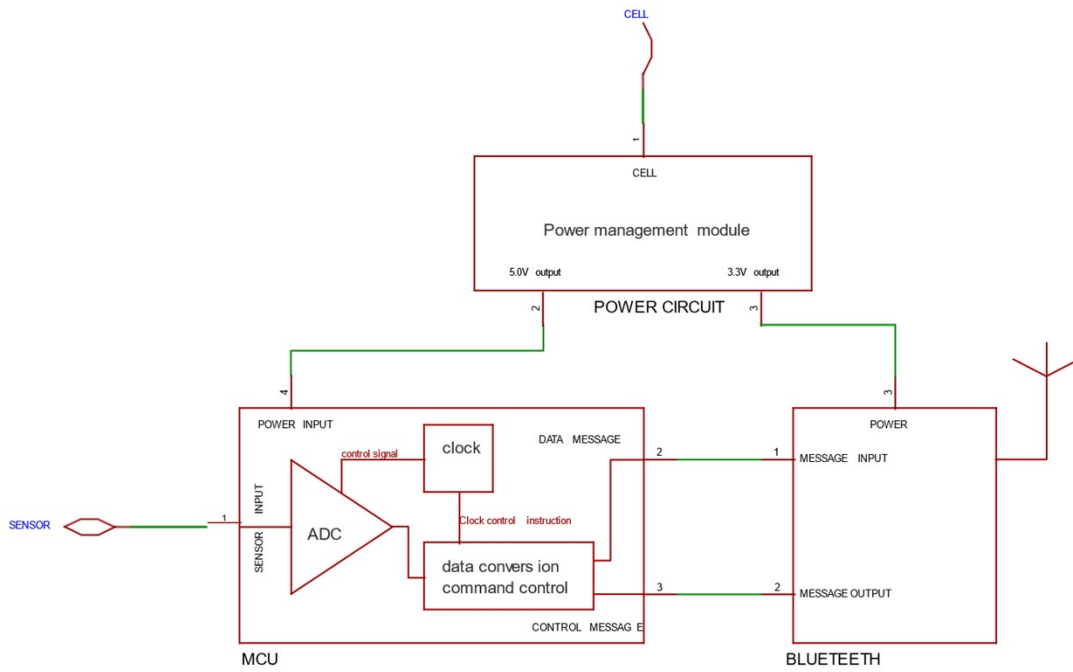


**Fig. S28.** Schematic diagram of signal-conditioning circuit.

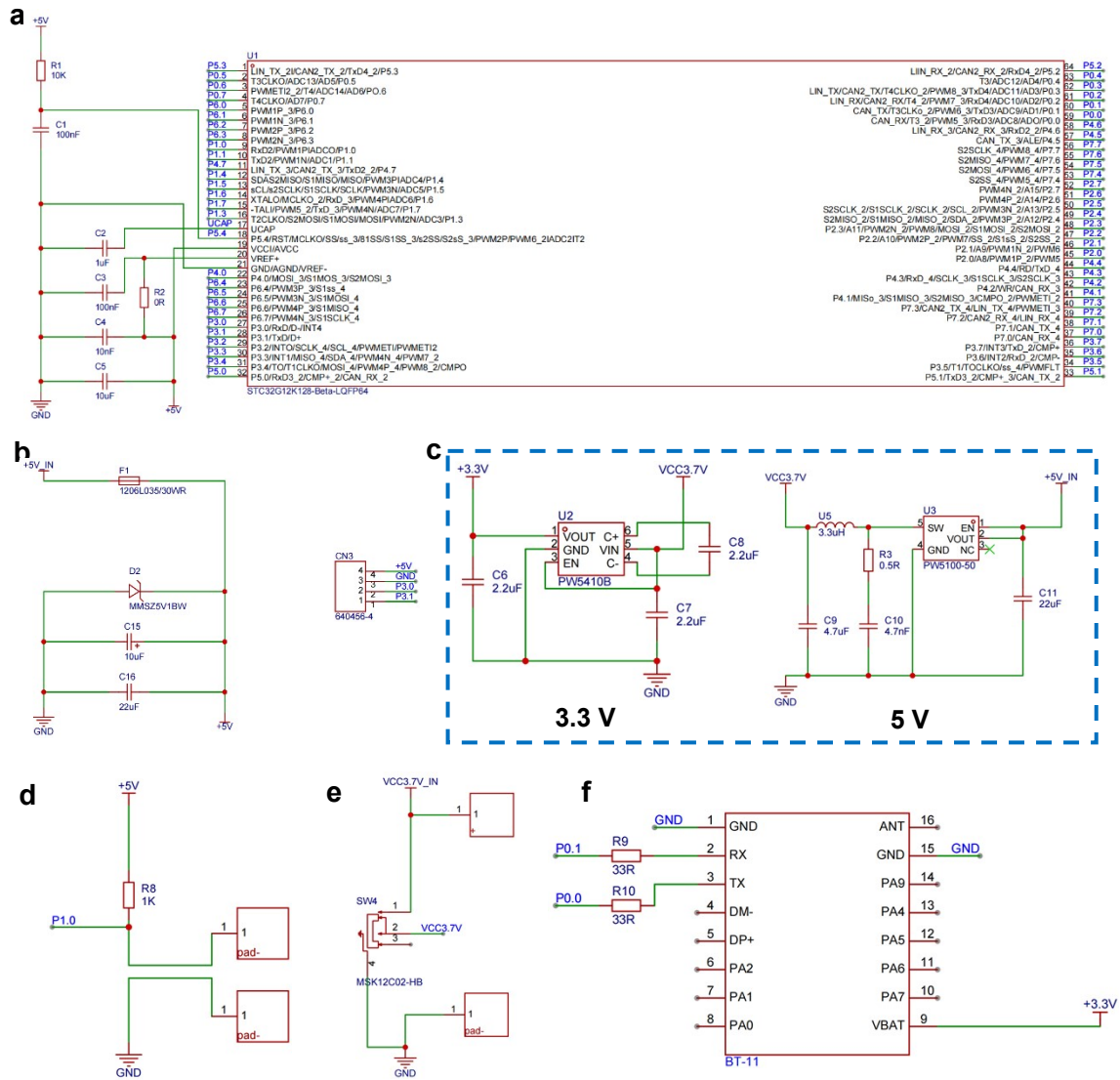


**Fig. S29.** Schematical diagram of PCB component circuit. (a) Single-chip microcomputer minimum system. (b) Program debugging interface. (c) Voltage stabilizer module. (d) Test circuit. (e) Power interface. (f) Bluetooth module.



**Fig. S30.** The photographs of the wearable sensing system for human motion monitoring: (a) bicep curl and (b) bike riding.

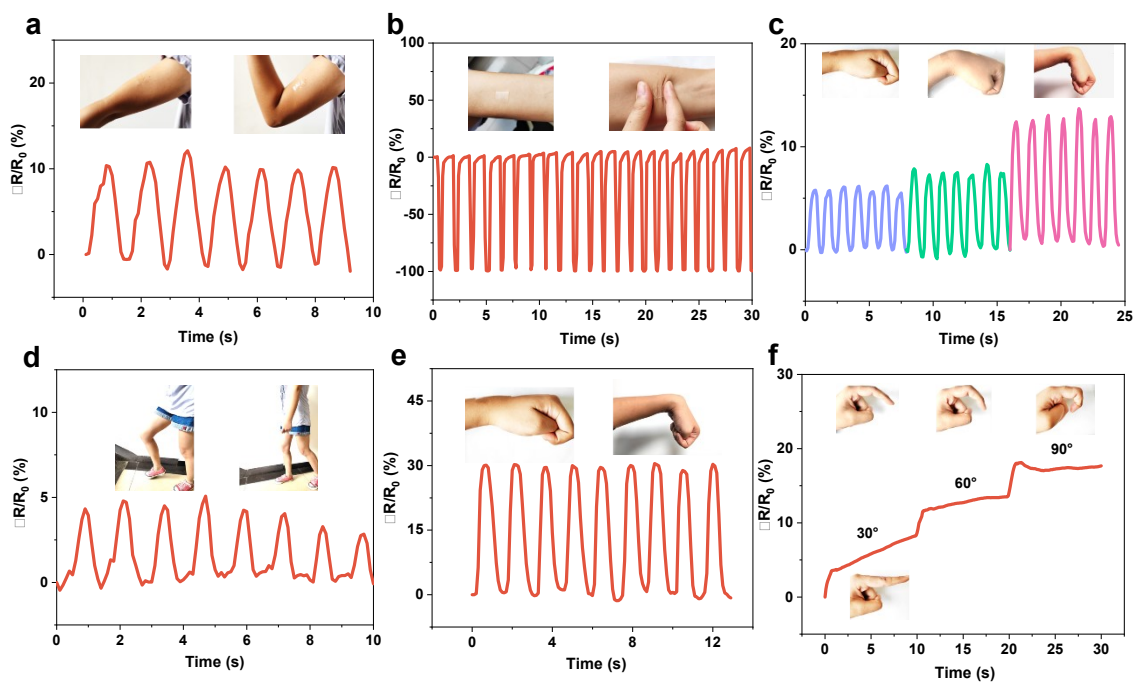


**Fig. S31.** The relative resistance response of the Ur-SA hydrogel sensor for various human motion monitoring: (a) elbow bending, (b) skin compressing, (c) wrist bending at different stretches, (d) walking, (e) wrist bending, (f) finger bending using the Ur-SA hydrogel sensor.